NARROW-BAND AND DERIVATIVE-BASED VEGETATION INDICES FOR HYPERSPECTRAL DATA

K. R. Thorp, L. Tian, H. Yao, L. Tang

ABSTRACT. *Hyperspectral remote sensing imagery was collected over a soybean field in central Illinois in mid-June 2001 before canopy closure. Estimates of percent vegetation cover were generated through the processing of RGB (red, green, blue) digital images collected on the ground with an automated crop mapping system. A comparative study was completed to test the ability of broad-band, narrow-band, and derivative-based vegetation indices to predict percent soybean cover at levels less than 70%. Though remote sensing imagery is commonly analyzed using reference data collected at random points over a scene of interest, the analysis of the hyperspectral imagery in this research was performed on a pixel-by-pixel basis over the field area covered by the automated crop mapping system. Narrow-band and derivative-based indices utilizing the finer spectral detail of hyperspectral data performed better than the older broad-band indices developed for use with multispectral data. Specifically, second-derivative indices measuring the curvature in the green region (514-556 nm), longer wavelength red region (640-694 nm), and short wavelength NIR (712-778 nm) performed well. Narrow-band indices, based on the standard ratio index equations, which used values from the blue (472-490 nm) and green (514-550 nm) regions, also performed well for many of the datasets. The performance of all indices was shown to suffer over areas of brighter soil background, and the use of ratio-based narrow-band indices that did not incorporate NIR reflectance values performed best in this case.*

Keywords. *Hyperspectral, Imagery, Image processing, Image segmentation, Index, Remote sensing.*

Vegetation indices have commonly been used to quantify amounts of vegetation present in reflectance data (Jordan, 1969; Ashley and Rea, 1975; Huete, 1988; Thenkabail et al., 2000). To date, most vegetation indices have been developed for use with multispectral remote sensing imagery and other reflectance data having a relatively broad bandwidth. With recent developments in hyperspectral technology, reflectance data can now be collected with a very high spectral resolution, much greater than that of the older multispectral data. The advent of this new technology has generated much interest in the development of new vegetation indices such that the greater spectral detail of hyperspectral data can be utilized. Recently, hyperspectral datasets have been used in the development of narrow-band vegetation indices (Thenkabail et al., 2000) and derivative-based vegetation indices (Tsai and Philpot, 1998). Narrow-band indices function similarly to the older broad-band indices; however, the range of reflectance values used in the index equations are refined to exploit the fine spectral detail in hyperspectral data. Derivative-based indices analyze the slope and curvature of reflectance curves rather than reflectance values themselves and have been most useful for analysis of the "red edge" in the spectral response of vegetation (Datt and Paterson, 2000).

Soil background has been shown to affect the performance of vegetation indices, and extensive research has been done to examine the characteristics of reflectance measured over partial canopies. Huete et al. (1985) concluded that standard vegetation indices improperly modeled the effect of soil brightness on partial canopy reflectance. Furthermore, soil brightness influences were found to increase with increasing canopy cover up to 60%, suggesting that soil and plant spectra collectively interact in a non-additive, nonlinear fashion to produce a composite spectral response. In a related experiment, Huete (1987) concluded that, in the case of significant canopy coverage, only a small portion of red radiation reaches the underlying soil surface due to intense absorption by chlorophyll. On the other hand, the plant leaves readily scatter and transmit near-infrared (NIR) radiation deep into the canopy. Therefore, since vegetation can differentially alter the intensity of radiant flux through the canopy, the spectral response of underlying soil will exhibit properties of both soil and vegetative reflectivity. Since soil brightness determines the magnitude of this unique soil response, it follows that errors in "greenness" measurements by vegetation indices depend on both the quantity of vegetation available for radiant flux differentiation and the brightness of underlying soil. For this reason, the development of soil-adjusted vegetation indices for vegetation

Article was submitted for review in October 2002; approved for publication by the Information & Electrical Technologies Division of ASAE in September 2003.

The use of trade names is only intended to provide specific information to the reader, and does not constitute endorsement by the University of Illinois.

The authors are **Kelly Robert Thorp, ASAE Member,** Graduate Research Assistant, **Lei Tian, ASAE Member Engineer,** Associate Professor, and **Haibo Yao, ASAE Member,** Graduate Research Assistant, Department of Agricultural Engineering, Illinois Laboratory for Agricultural Remote Sensing, University of Illinois at Urbana-Champaign, Urbana, Illinois; and **Lie Tang,** Assistant Professor, Department of Agrotechnology and Food Sciences, Wageningen University, Wageningen, The Netherlands. **Corresponding author:** Lei Tian, Department of Agricultural Engineering, 1304 W. Pennsylvania Avenue, University of Illinois at Urbana-Champaign, Urbana, IL 61801; phone: 217-333-7534; fax: 217-244-0323; e-mail: lei-tian@uiuc.edu.

assessments over variable soil backgrounds has also been an important goal in remote sensing research (Huete, 1988; Rondeaux et al., 1996).

Objective

The objective of this study was to develop narrow-band and derivative-based vegetation indices for hyperspectral data and test their ability to accurately measure soybean canopy coverage at levels less than 70%. The performance of these indices was contrasted to that of older broad-band indices, such as the normalized difference vegetation index (NDVI). In addition, the effect of soil background on index performance was studied.

Materials and Methods

Data collection occurred over an 11.3 ha (28 acre) section of a production soybean (*Glycine max* (L.) Merr.) field near Mahomet, Illinois, as shown in figure 1. The primary soil types for the study region included Drummer, Dana, Raub, and Wyanet, which are all high-yielding, silt-loam soils typical for the central Illinois area. On May 5, 2001, glyphosate-tolerant soybeans were planted at a 38.1 cm (15 in.) spacing in no-till corn (*Zea mays* L.) residue. Aerial remote sensing imagery was collected over the study area using Spectral Visions' RDACS-H3 aerial hyperspectral focal plane scanner (Mao, 2000), which could collect either 60 or 120 bands of reflectance data over the range of 472 to 826 nm. This corresponded to a 6 nm bandwidth for 60-band images and a 3 nm bandwidth for 120-band images. Sixty-band imagery of 0.5-meter spatial resolution was collected for calculation of vegetation indices on June 13, 2001, while 120-band imagery at 2-meter spatial resolution was collected for the analysis of the soil background on April 24, 2001.

Ground reference data was collected on June 17, 2001, using the real-time variable-rate application and crop mapping system developed by Tang (2002). The system incorporated two RGB cameras and positioning equipment for automatic, sequential collection of RGB digital images over the crop canopy as the vehicle, a Tyler Patriot XL-772 agricultural sprayer, traveled through the field. Throughout image acquisition, a medium-accuracy global positioning system (GPS) receiver was used to record the geographic location of the center point for each RGB image. Locations for ground reference data collection were determined based on the design of a variable-rate herbicide application experiment that was carried out concurrently with data collection for this experiment. A total of 12 sprayer passes were successfully mapped. Each pass contained approximately 60 images that covered a 2.4×3.0 square meter (8×10 square foot) area on the ground. A total of 718 images covering 0.53 ha (1.32 acres) of field area were collected. Laboratory analysis of these images at a later time provided a large volume of ground reference information for use in the analysis of vegetation indices for hyperspectral data.

Ground-Reference Image Processing

As described by Tang et al. (2002), a genetic algorithm-based, supervised color image segmentation in the HSI (hue, saturation, intensity) color space was used to separate plants (crop and weeds) from the background (soil, rocks, and residue) for his real-time, machine-vision-based, in-field variability mapping and selective herbicide application system. This algorithm was also used to generate measurements of percent vegetation cover from the ground images in this experiment. Before running the segmentation algorithm, an environmentally adaptive look-up table (LUT) procedure (Tian and Slaughter, 1998) was used to describe the range of values in HSI color space that represented vegetation in the images. The overall performance of the segmentation was heavily dependent on a proper choice of values for the LUT, which could vary depending on lighting conditions, soil color, residue cover, and greenness of vegetation. LUTs were optimized for each pass using an interactive routine developed by Tang (2002) that allowed the user to select "green" pixels representing vegetation in the image. The HSI color range of the selected pixels then became the new LUT for vegetation segmentation. The algorithm was programmed to

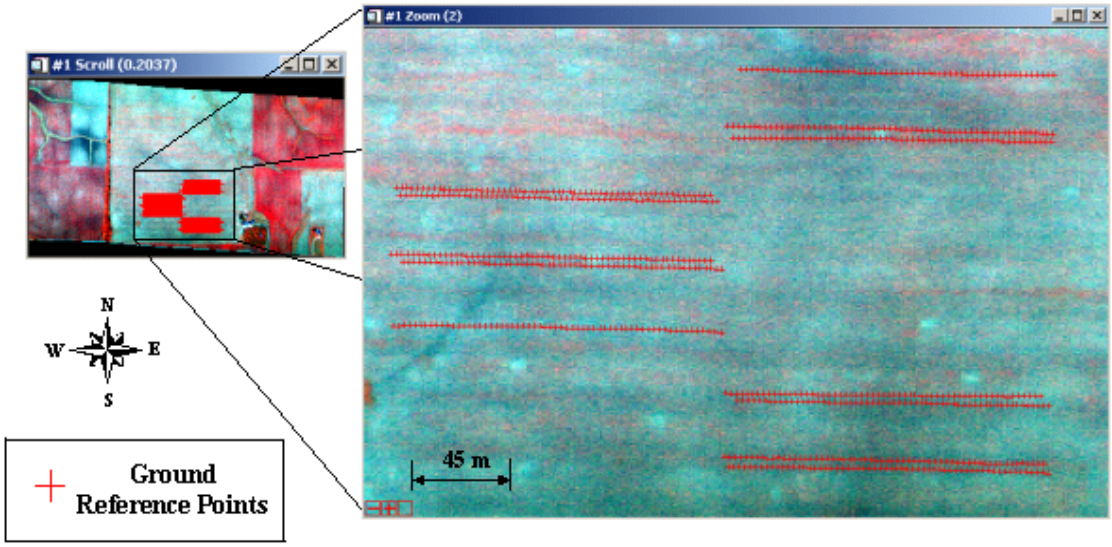

Figure 1. Data collection over the study site. RGB digital images were collected in 12 passes of an automatic data collection system. Image locations are overlaid on this 1-meter resolution hyperspectral image (June 13, 2001).

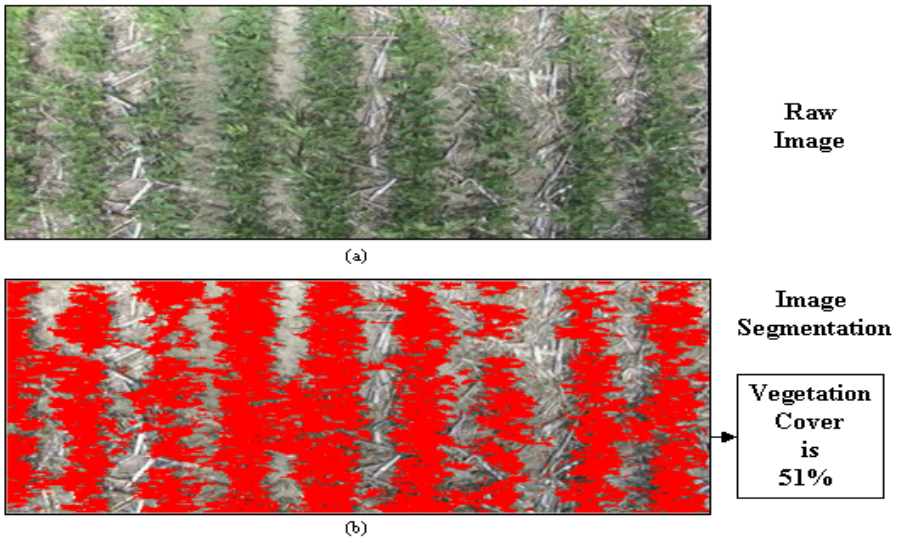

Figure 2. Ground reference image segmentation: (a) ground reference images were (b) processed using a genetic algorithm-based, supervised color image segmentation in HSI color space to generate an estimate for vegetation cover at each ground image location.

segment all the images from a single sprayer pass as a batch process, each with a specifically tailored LUT. Figure 2 shows a ground image with its processed result.

Hyperspectral Image Processing

A variety of preprocessing steps was performed to prepare the hyperspectral imagery for analysis, including both spatial and spectral modifications. First, since raw-image spatial distortions can be produced by roll, pitch, and yaw of the aircraft during the scanner-based image collection process, a correction procedure, developed by Yao et al. (2001), was implemented to remove as much raw distortion in the hyperspectral imagery as possible. Next, the images were georeferenced to the Universal Transverse Mercator (UTM) coordinate system using a variety of coordinate references including a field boundary map and a USGS digital orthoquad. For spectral correction, a minimum noise fraction (MNF) transformation (Green et al., 1988) was used to remove noise in the raw reflectance data. The imagery was then calibrated to percent reflectance using the reflectance measurements from ground-level radiometric targets in an empirical line calibration procedure (Smith and Milton, 1999).

After the initial processing steps were completed for both the ground reference dataset and the hyperspectral images, a routine was developed for extraction of spectral data from the imagery at the location of each ground reference image. In this way, vegetation indices could be calculated from the spectral information at each ground reference location, and a correlation coefficient (r) could be calculated to relate vegetation index calculations to measures of percent canopy coverage from the ground-based images. To carry out this objective, a routine was developed using the Interactive Data Language (IDL). Extra care was taken to ensure that the area of spectral information extracted from the hyperspectral imagery most accurately represented the area covered by the ground-based images. For example, ground images were usually more centered over spectral data extraction regions with odd dimensions. In addition, higher resolution imagery allowed for better centering of ground images over the spectral data extraction region. For the 0.5-meter imagery used in this analysis, the ground reference images were most accurately overlaid on extraction regions covering a 5×6 pixel area. For further details on the spectral data extraction process, see Thorp (2002) or Thorp et al. (2002).

Analysis of Vegetation Indices

Reflectance data extracted from the 5×6 regions of interest in the 0.5-meter hyperspectral imagery were averaged to generate a single reflectance curve for each region. Using the average spectral response for each region, a variety of vegetation indices was calculated for a comparative analysis. These included the older broad-band indices developed for use with multispectral datasets, narrow-band indices that utilized the finer spectral resolution of hyperspectral images, and derivative indices that focused on the slope and curvature of the reflectance curves rather than the actual reflectance values themselves. To analyze the performance of the indices, r was calculated to determine the relationship between the index values and the canopy coverage estimates from the ground-based images. Coefficients were calculated separately for each sprayer pass and collectively for the entire ground reference dataset. In addition, since the performance of vegetation indices has been shown to vary based on soil background (Heute et al., 1985) and since these datasets were collected prior to canopy closure, the ground reference dataset was also divided according to soil background for further analysis.

Division of Ground Reference Data According to Soil Background

Two methods were attempted to define the location of different soil backgrounds over the study area, so the ground reference data could be divided accordingly. First, a second-order digital soil survey of the study area was obtained, and the ground reference data were separated by soil type using a geographic information system (GIS). However, since the soil survey was generated through the interpolation of soil samples collected on a 0.4 ha (1 acre) grid, the resolution of the survey was not high enough for accurate division of the high-density ground reference data by soil type. Therefore,

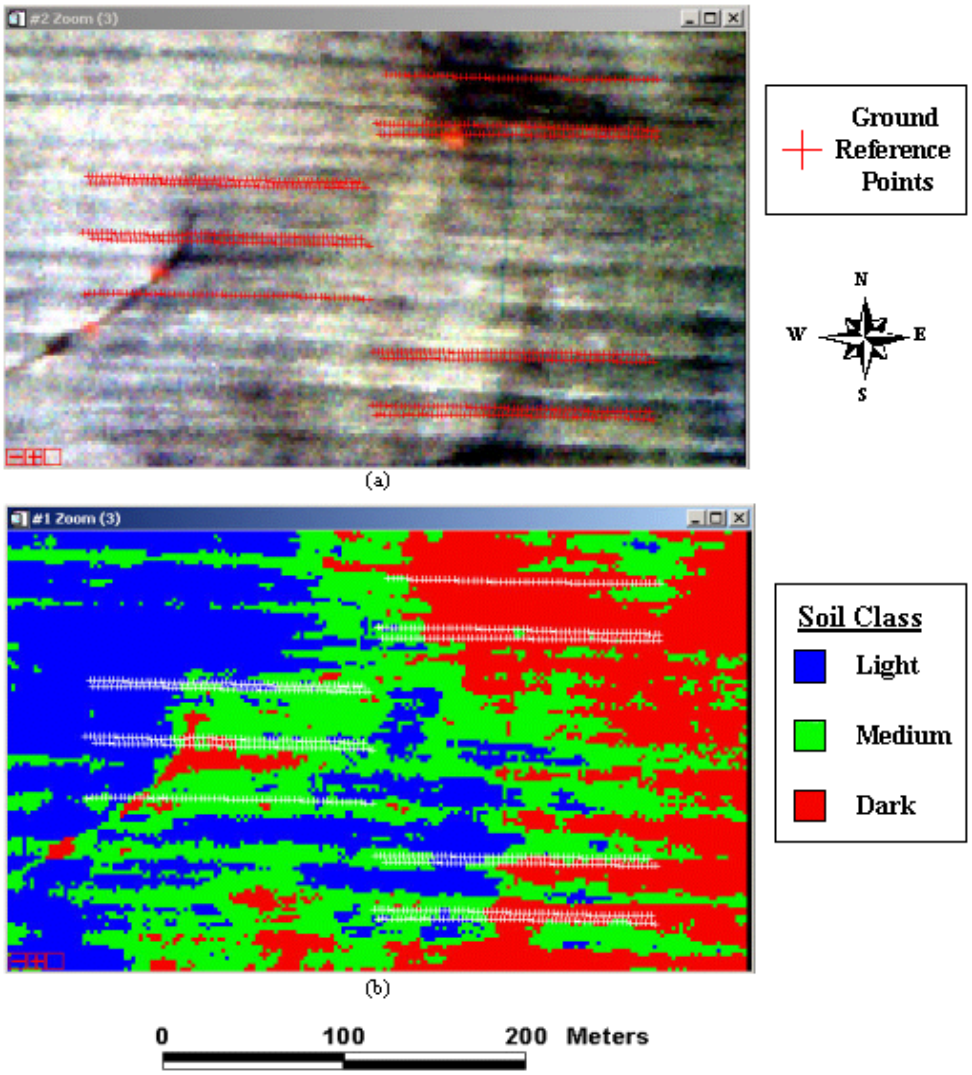

Figure 3. Bare soil image classification. An unsupervised classification algorithm was used to divide this (a) bare soil hyperspectral image (April 24, 2001) into (b) three soil classes, and this result was used to divide the ground reference dataset according to soil reflectance properties.

a better approach, which involved an unsupervised classification of a bare soil hyperspectral image over the study site, was attempted. On April 24, 2001, a 120-band bare soil hyperspectral image at 2.0-meter spatial resolution was collected over the study site. After preprocessing steps were completed for this imagery, an unsupervised classification algorithm was used to divide the bare soil imagery into three spectral classes, labeled light, medium, and dark. Based on the result of the classified bare soil image, the ground reference data were divided according to soil reflectance, such that vegetation index performance could be analyzed according to soil reflectance properties. The bare soil image over the study area along with its classified result are shown in figure 3.

Calculation of Broad-Band Vegetation Indices

To generate estimates for broad-band reflectance, the hyperspectral reflectance values over a range of wavelengths were averaged together. Similar to the approach used by Thenkabail et al. (2000), hyperspectral wavebands from 760 nm to 826 nm were averaged to generate an NIR broad band, and the wavebands from 634 nm to 688 nm were averaged to generate a red broad band. With these simulated broad-band reflectance values, six broad-band vegetation indices, including the difference vegetation index (DVI), the ratio vegetation index (RVI), the NDVI, the soil-adjusted vegetation index (SAVI), the modified soil-adjusted vegetation index (MSAVI), and the optimized soil adjusted vegetation index (OSAVI), were calculated from the reflectance data extracted at each ground reference location. A summary of the index equations can be found in table 1. For each ground reference dataset, the resulting broad-band index calculations were then correlated to the vegetation cover measurements from the ground-based images. The results of this correlation analysis are given in the APPENDIX.

Development and Calculation of Narrow-Band Vegetation Indices

To develop a set of narrow-band vegetation indices, a technique was borrowed from Thenkabail et al. (2000). Since a total of 60 discrete spectral bands from 472 nm to 826 nm were available in the 0.5-meter imagery, the six broad-band equations in table 1 were used to calculate index values for all possible two-band combinations of the 60 discrete bands (1770 useful combinations) using reflectance values extracted from the 5×6 regions of interest. Coefficients were

Table 1. Broad-band vegetation indices (λ_{NIR} is the broad-band near-infrared reflectance, and λ_{red} is the broad-band red reflectance).

Index	Equation	Reference
DVI	$DVI = (\lambda_{NIR} - \lambda_{red})$	Tucker (1979)
RVI	$RVI = \frac{\lambda_{NIR}}{\lambda_{red}}$	Jordan (1969)
NDVI	$NDVI = \frac{(\lambda_{NIR} - \lambda_{red})}{(\lambda_{NIR} + \lambda_{red})}$	Ashley and Rea (1975)
SAVI	$SAVI = \frac{(\lambda_{NIR} - \lambda_{red})}{(\lambda_{NIR} + \lambda_{red} + L)} \cdot (1 + L)$	Huete (1988)
MSAVI	$MSAVI = \frac{2\lambda_{NIR} + 1 - \sqrt{(2\lambda_{NIR} + 1)^2 - 8(\lambda_{NIR} - \lambda_{red})}}{2}$	Qi et al. (1994)
OSAVI	$OSAVI = \frac{(\lambda_{NIR} - \lambda_{red})}{(\lambda_{NIR} + \lambda_{red} + 0.16)}$	Rondeaux et al. (1996)

then calculated to find the strength of the linear correlation between the index values and the corresponding vegetation cover measurements. Contour plots, such as the one shown in figure 4, were constructed to find the two-band combinations that produced the highest correlation with vegetation cover for each ground reference dataset. For all indices and for all datasets, the contour plots showed a general trend similar to that in figure 4. Namely, there were four areas in the contour plots where the *r* for two-band indices and vegetation cover were always higher. This indicated a potential for the development of four narrow-band vegetation indices using the wavelengths at these areas. Through a visual inspection of the contour plot for each ground reference dataset, the optimum range of wavelengths to be used for narrow-band index calculations was found. A summary of the chosen wavelength ranges is given in table 2.

The validity of these narrow-band indices can be explained as they relate to vegetative reflectance properties. Index 1 uses a portion of longer wavelength blue light (472 to 490 nm) and the portion of the green spectrum associated with the increased reflectance of green light from chlorophyll (514 to 550 nm). The index contrasts the wavelengths of maximum green light reflectance to that of maximum blue light absorbance. Index 2 involves a portion of longer red wavelengths (646 to 670 nm) and a portion of wavelengths between green and red light (586 to 616 nm). This index measures the absorbance of longer wavelength red light as it varies with changes in pigment content. Moreover, index 2 progresses from positive to negative values as more red light is absorbed. Index 3 contrasts the longer portion of red wavelengths (646 to 676 nm) with the wavelengths associated with the red edge (700 to 736 nm). With increasing vegetation cover, red reflectance drops and the steepness of the red edge increases, creating a greater contrast at these wavelengths. Index 4 utilizes the wavelengths most commonly associated with the older broad-band indices. For this index, a portion of the longer wavelength red region (652 to 688 nm) and a portion of the shorter NIR wavelengths (754 to 820 nm) were used. After the development of the optimum two-band combinations, hyperspectral wavebands were

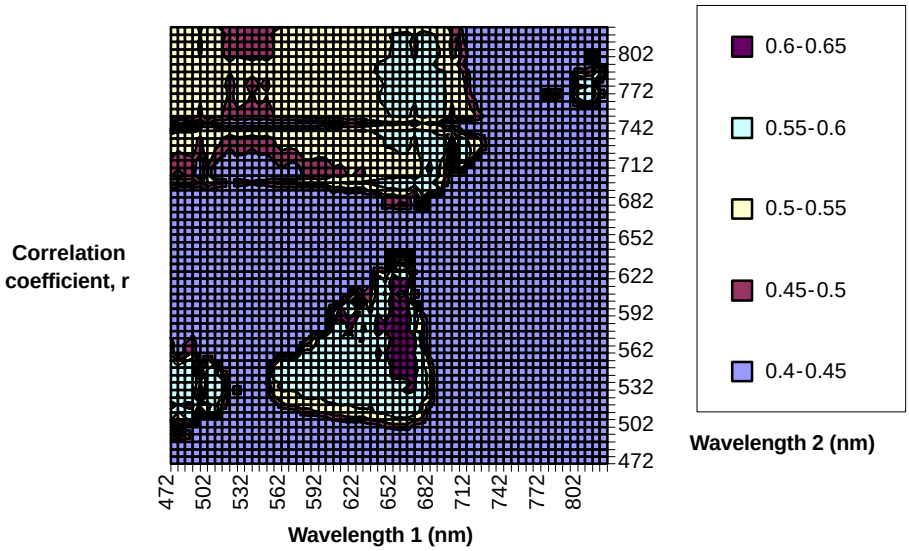

Figure 4. Correlation coefficients for the narrow-band MSAVI and vegetation cover for all ground data. Contour plots such as these were used for finding band combinations most highly correlated to vegetation cover. Correlation coefficients less than 0.45 were set to zero for easier interpretation of the best bands.

Table 2. Summary of wavelengths chosen for two-band index calculations using narrow bands. The wavelength ranges were chosen through a visual inspection of the contour plots, such as that in figure 4.

	Index 1	Index 2	Index 3	Index 4
Wavelength range 1 (nm)	472-490	646-670	646-676	652-688
Wavelength range 2 (nm)	514-550	586-616	700-736	754-820

averaged over the optimum ranges, and each of the four combinations was used in the calculation of narrow-band indices using the DVI, RVI, NDVI, SAVI, MSAVI, and OSAVI equations. Since the four narrow-band wavelength ranges were used in six broad-band equations, a total of 24 narrow-band indices were calculated. The resulting index values were then correlated to the measures of vegetation cover for each of the ground reference dataset divisions described previously. The results of this analysis are found in the APPENDIX.

Development and Calculation of Derivative-Based Indices

The final vegetation index calculations for the reflectance data in this study were derivative-based. To perform the derivative analysis, methods were adopted from Tsai and Philpot (1998), who applied the Savitzky and Golay (1964) convolution method for data smoothing and derivative calculations to reflectance data. Using the Savitzky-Golay method, shaped filter windows were convolved across the bands of reflectance data to both smooth the data and calculate derivatives at the same time in one pass of the filter. Since Tsai and Philpot (1998) showed that the size of the convolved filter had the greatest effect on the degree of spectral smoothing, various filter sizes were tested to determine the size that provided the optimum noise removal without significant elimination of useful signal. To support their convolution method, Savitzky and Golay (1964) provided tables of coefficients to be used for various sizes of filter windows. Later, Madden (1978) developed equations from which filter window coefficients for the zeroth to fifth order derivatives could be calculated. A C++ program incorporating Madden's (1978) equations was developed so that filter window coefficients could be calculated for various filter sizes. After making these calculations, the program then convolved the resulting filter across the reflectance data extracted from the 0.5-meter hyperspectral imagery. Through a visual assessment of the resulting derivative curves, an optimum filter size of 9 was chosen for the first derivative by determining the smallest filter that provided a smooth derivative curve. Similarly, a filter size of 15 was chosen for the second derivative. A larger filter was required for the second derivative because the noise in the original signal was further magnified by the higher order derivative.

Once the optimum filter sizes were determined, the first and second derivatives of the extracted hyperspectral reflectance data were calculated. Examples of the calculated first and second derivatives for a typical reflectance curve in this dataset are shown in figure 5. The first derivative curve contained two distinct peaks. The first, centered at 514 nm, corresponded to the point of maximum slope as the reflectance increased in the green portion of the visible spectrum. The second, centered at 700 nm, corresponded to the point of maximum slope at the red edge where the low red reflectance increased to the high NIR reflectance. For the second derivative curves, three distinct peaks existed. The first, centered at 532 nm, corresponded to the wavelength at which the reflectance reached a maximum in the green portion of the visible spectrum. The second, centered at 676 nm, corresponded to the point of maximum curvature in the longer red wavelengths as the reflectance began to rise toward the red edge. The third, centered at 730 nm, indicated the point at the red edge where the reflectance values began to level off in the NIR region.

Derivative vegetation indices have been calculated by integrating the area underneath the peaks in the derivative curves (Chen et al., 1993). A similar method was adopted here. To find the optimum integration range, derivative calculations at each wavelength were correlated to the ground reference vegetative cover measurements, and the optimum integration ranges were chosen from wavelengths whose derivative values were most highly correlated to vegetation cover. Table 3 shows the wavelength ranges used for calculation of derivative indices in this research. Once the optimum wavelength ranges were chosen, derivative vegetation indices were calculated by integrating the area under the first and second derivative curves for reflectance data extracted from the 5×6 regions of interest. The resulting index values were then correlated to the measurements of vegetation cover for each ground reference dataset, as shown in the APPENDIX.

RESULTS AND DISCUSSION

Results of the index analysis are shown in the APPENDIX, where the top index for each dataset is highlighted in boldface. For each vegetation index, r was calculated for each division of the ground data, including each sprayer pass, soil type, and soil reflectance class. A final r was calculated for each index using the entire ground reference dataset as a whole. For the broad-band indices, the DVI most commonly provided the highest r with vegetation cover measurements. Except for the DVI, all broad-band indices tested in this study were ratio-based indices. Huete et al. (1985) determined that ratio-based indices performed best at vegetation covers greater than 70%, and that non-ratio-based indices such as the DVI performed best for lower vegetation covers. Since no vegetation cover measurements were greater than 70% in this study, the results of Huete et al. (1985) concerning the better performance of the DVI at lower vegetation covers were confirmed. In addition, there was no significant difference in the performance of soil-adjusted indices and non-soil-adjusted indices in this research.

For the ratio-based, narrow-band indices, index 1 performed the best. This index contrasted the high absorbance of blue (472 to 490 nm) light to the maximum reflectance of visible light in the green (514 to 550 nm) region, but the index calculation surprisingly did not include any reflectance measurements in the NIR region, a common requirement for most broad-band indices. From this, it can be speculated that, because vegetation cover in the field was moderate, the varying degree of vegetation-scattered NIR radiation reflected by the soil negatively affected the performance of the ratio-based indices requiring NIR reflectance measurements. As a result, the use of an index requiring only the reflectance of visible light worked better, because the high absorbance of light by vegetation at these wavelengths reduced the potential for variable reflection of vegetation-transmitted radiation by the soil background. For the non-

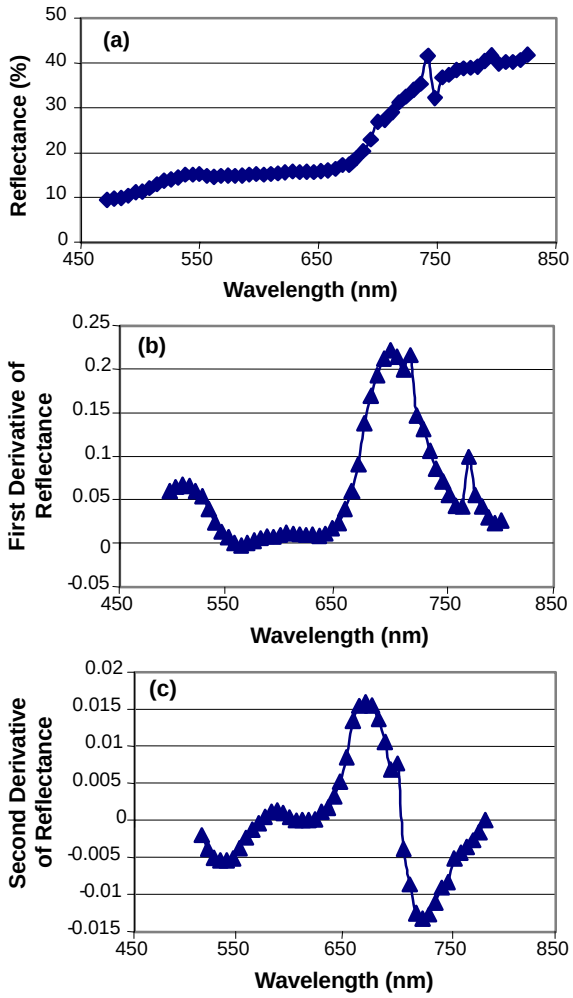

Figure 5. (a) Typical reflectance curve in this dataset with its (b) first and (c) second derivative curves. First and second derivatives were calculated using Savitzky-Golay smoothing and differentiation with filter windows of size 9 and 15, respectively.

Table 3. Wavelength ranges over which the derivative curves were integrated to calculate derivative-based vegetation indices. Ranges represent the wavelengths whose derivative values were most highly correlated to vegetation cover.

	Wavelength Range 1	Wavelength Range 2	Wavelength Range 3
First derivative	496-520	670-742	--
Second derivative	514-556	640-694	712-778

ratio-based DVI, the best narrow-band indices were index 3 and index 4, which both included measurements of NIR radiation. This confirmed that the results of Huete et al. (1985), concerning the better performance of broad-band, non-ratio-based indices at lower vegetation covers, could also be applied to narrow-band, non-ratio-based indices.

For the derivative indices, the second derivative generally performed better than the first derivative. This supported previous results that the second derivative removes more of the soil background effects than the first derivative (Datt and Paterson, 2000). However, the best range for calculating a derivative-based index could not be concluded because the results between the tested wavelength ranges for the second derivative were not significantly different. Perhaps a single index involving a combination of the three wavelength ranges used in the second derivative analysis should be developed.

Division of the ground reference dataset according to soil background provided some interesting results. The most concrete conclusions could be drawn through the division of ground reference data according to soil reflectance. In this case, for all indices, *r* decreased as soil brightness increased. Vegetation indices performed better over darker soils because the dark soil background contributed less strongly to the overall spectral signal, and the vegetation signal-to-noise ratio was higher in these areas. In addition, the narrow-band, ratio-based index 1, which contained no NIR reflectance measurements, performed the best for both the light and medium colored soils. This result further supported the notion that the reflectance of vegetation-scattered NIR radiation from soil negatively affected the performance of vegetation indices requiring NIR reflectance measurements. Furthermore, since the index requiring no NIR reflectance value performed the best over the light and medium soil colors, vegetation-transmitted NIR must be reflected more strongly from brighter soils than darker soils. For the darker soil color, the narrow-band DVI index 3, which did use NIR reflectance, performed the best. This indicated that vegetation-transmitted NIR radiation was reflected less strongly from the dark soil. It was concluded that the divisions of the ground data by soil reflectance provided more meaningful results than the divisions by soil type, because correlation results for divisions by soil type seemed to be more dependent on the sample size of data points in each soil type class.

Conclusion

When compared to the *r* for the best performing broad-band index, *r* was increased by an average of 6.3% when using narrow-band indices and by an average of 4.6% when using derivative-based indices. However, the best performing narrow-band or derivative-based indices were not consistent between datasets, and it is not possible to select a single index that consistently outperformed other indices. Instead, several indices were chosen to be adequate performers. These included the narrow-band, ratio-based index 1 that contrasted blue (472 to 490 nm) light absorbance to green (514 to 550 nm) light reflectance. In addition, the narrow-band DVI index 3, which utilized the longer wavelength red (646 to 676 nm) reflectance and the reflectance associated with the red edge (700 to 736 nm), performed well. The second derivative indices also tended to perform well. These indices measured the curvature in the green (514 to 556 nm) region, in the longer wavelength red (640 to 694 nm) region, and in shorter wavelength NIR (712 to 778 nm). Though these indices performed better than the older broad-band indices in general, the performance of all indices was shown to vary based on soil reflectance properties. As soil brightness increased, a decrease in the ability to measure vegetation cover using any of the tested vegetation indices was seen. In addition, the ratio-based, narrow-band indices that employed blue (472 to 490 nm) and green (514 to 550 nm) radiation, but no NIR reflectance measurements, performed better over areas of partial canopy coverage than the ratio-based, narrow-band indices that did utilize NIR reflectance. This indicated that the reflectance of vegetation-transmitted NIR radiation from soil greatly hindered the

performance of ratio-based indices. On the other hand, for the non-ratio-based DVI, NIR reflectance measurements were required for optimum performance. Finally, the study showed that further development is necessary to prevent soil effects from influencing the result of vegetation index calculations.

ACKNOWLEDGEMENTS

This material is based on work supported by the United Soybean Board under Award No. SBA-USB-1248 and the University of Illinois. In addition, a special thanks is given to the Institute of Technology Development/Spectral Visions and NASA for collection of hyperspectral imagery. Any opinions, findings, and conclusions or recommendations expressed in this publication are those of the authors and do not necessarily reflect the views of the United Soybean Board or the University of Illinois.

REFERENCES

Ashley, M. D., and J. Rea. 1975. Seasonal vegetation differences from ERTS imagery. *Photogrammetric Eng. and Remote Sensing* 41(6): 713-719.

Chen, Z., C. D. Elvidge, and W. T. Jansen. 1993. Description of derivative-based high spectral-resolution (AVIRIS) green vegetation index. In *Proc. SPIE: Imaging Spectroscopy of the Terrestrial Environment* 1937: 43-54. G. Vane, ed.

Datt, B., and M. Paterson. 2000. Vegetation-soil spectral mixture analysis. In *Proc. IEEE International Geoscience and Remote Sensing Symposium (IGARSS)* 5: 1936-1938.

Green, A. A., M. Berman, P. Switzer, and M. D. Craig. 1988. A transformation for ordering multispectral data in terms of image quality with implications for noise removal. *IEEE Trans. Geoscience and Remote Sensing* 26(1): 65-74.

Huete, A. R. 1987. Soil-dependent spectral response in a developing plant canopy. *Agronomy J.* 79(1): 61-68.

Huete, A. R. 1988. A soil-adjusted vegetation index (SAVI). *Remote Sensing of Environment* 25(3): 295-309.

Huete, A. R., R. D. Jackson, and D. F. Post. 1985. Spectral response of a plant canopy with different soil backgrounds. Remote Sensing of Environment 17(1): 37-53.

Jordan, C. F. 1969. Derivation of leaf-area index from quality of light on the forest floor. Ecology 50(4): 663-666.

Madden, H. H. 1978. Comments on the Savitzky-Golay convolution method for least-squares fit smoothing and differentiation of digital data. Analytical Chemistry 50(9): 1383-1386.

Mao, C. 2000. Hyperspectral focal plane scanning: An innovative approach to airborne and laboratory pushbroom hyperspectral imaging. In Proc. 2nd International Conference on Geospatial Information in Agriculture and Forestry, Vol 1: 424-428. Ann Arbor, Mich.: ERIM International, Inc.

Qi, J., A. Chehbouni, A. R. Huete, Y. H. Kerr, and S. Sorooshian. 1994. A modified soil adjusted vegetation index. Remote Sensing of Environment 48(2): 119-126.

Rondeaux, G., M. Steven, and R. Baret. 1996. Optimization of soil-adjusted vegetation indices. *Remote Sensing of Environment* 55(2): 95-107.

Savitzky, A., and M. J. E. Golay. 1964. Smoothing and differentiation of data by simplified least squares procedures. *Analytical Chemistry* 36(8): 1627-1639.

Smith, G. M., and E. J. Milton. 1999. The use of the empirical line method to calibrate remotely sensed data to reflectance. *International J. Remote Sensing* 20(13): 2653-2662.

Tang, L. 2002. Machine vision systems for real-time plant variability sensing and in-field application. PhD diss. Urbana, Ill.: University of Illinois at Urbana-Champaign, Department of Agricultural Engineering.

Tang, L., B. Steward, and L. Tian. 2000. Machine vision-based high-resolution weed mapping and patch-sprayer performance simulation. *SAE Trans., J. Commercial Vehicles* 108(2): 317-326.

Tian, L., and D. C. Slaughter. 1998. Environmentally adaptive segmentation algorithms for outdoor machine vision systems. *J. Computers and Electronics in Agric.* 21(3): 153-168.

Thenkabail, P. S., R. B. Smith, and E. DePauw. 2000. Hyperspectral vegetation indices and their relationships with agricultural crop characteristics. *Remote Sensing of Environment* 71(2): 158-182.

Thorp, K. R. 2002. Variable-rate applications of herbicide using weed maps generated from remote sensing imagery. MS thesis. Urbana, Ill.: University of Illinois at Urbana-Champaign, Department of Agricultural Engineering.

Thorp, K. R., L. Tian, H. Yao, and L. Tang. 2002. Development of vegetation indices for hyperspectral data. ASAE Paper No. 021077. St. Joseph, Mich.: ASAE.

Tsai, F., and W. Philpot. 1998. Derivative analysis of hyperspectral data. *Remote Sensing of Environment* 66(1): 41-51.

Tucker, C. J. 1979. Red and photographic infrared linear combinations for monitoring vegetation. *Remote Sensing of Environment* 8(2): 127-150.

Yao, H., L. Tian, and N. Noguchi. 2001. Hyperspectral imaging system optimization and image processing. ASAE Paper No. 011105. St. Joseph, Mich.: ASAE.

See next page for APPENDIX.

APPENDIX

Results of the vegetation index analysis. Vegetation cover measurements were divided according to sprayer pass, soil type, and soil reflectance for the calculation of correlation coefficients with indices, and a final correlation was made using the entire ground reference dataset minus two passes that did not appear in the 0.5-meter imagery. The top coefficients for each dataset are highlighted in boldface.

	Sprayer Pass										Soil Type				Soil Reflectance			All Data
	1	2	3	4	5	6	7	8	9	10	Dana	Drmr	Raub	Wynt	L	M	D	
Sample Size	59	61	59	59	60	60	60	61	59	59	438	90	49	20	145	264	223	598
Broad band																		
DVI	**0.91**	**0.80**	0.75	0.28	0.73	0.83	0.72	0.68	0.67	0.83	0.57	0.85	0.88	0.92	0.41	0.56	0.80	0.59
RVI	0.73	0.64	0.77	0.22	0.75	0.71	0.66	0.69	0.40	0.63	0.61	0.77	0.75	0.92	0.46	0.59	0.70	0.57
NDVI	0.73	0.66	0.76	0.20	0.73	0.72	0.67	0.71	0.39	0.62	0.62	0.77	0.75	**0.93**	0.46	0.60	0.70	0.56
SAVI	0.73	0.66	0.76	0.20	0.73	0.72	0.67	0.71	0.39	0.62	0.62	0.77	0.75	**0.93**	0.46	0.60	0.70	0.56
MSAVI	0.73	0.66	0.76	0.20	0.73	0.73	0.67	0.72	0.38	0.62	0.62	0.77	0.75	**0.93**	0.47	0.60	0.69	0.55
OSAVI	0.73	0.66	0.76	0.20	0.73	0.72	0.67	0.71	0.39	0.62	0.62	0.77	0.75	**0.93**	0.46	0.60	0.70	0.56
Narrow band																		
DVI index 1	0.89	0.62	0.48	0.12	0.11	0.49	0.68	0.78	0.42	0.26	0.44	0.86	0.65	0.66	0.41	0.51	0.80	0.47
RVI index 1	0.81	0.74	**0.82**	0.29	0.75	0.78	0.78	**0.85**	0.78	**0.89**	0.69	0.84	0.90	0.89	**0.53**	0.68	0.78	0.59
NDVI index 1	0.82	0.75	**0.82**	0.29	0.75	0.78	**0.79**	**0.85**	0.78	**0.89**	0.69	0.84	0.90	0.89	**0.53**	0.68	0.77	0.59
SAVI index 1	0.82	0.75	**0.82**	0.29	0.74	0.78	**0.79**	**0.85**	0.78	**0.89**	**0.70**	0.84	**0.91**	0.89	**0.53**	**0.69**	0.78	0.59
MSAVI index 1	0.83	0.75	**0.82**	0.29	0.74	0.78	**0.79**	**0.85**	0.78	**0.89**	**0.70**	0.84	**0.91**	0.89	**0.53**	**0.69**	0.78	0.59
OSAVI index 1	0.82	0.75	**0.82**	0.29	0.75	0.78	**0.79**	**0.85**	0.78	**0.89**	**0.70**	0.84	0.90	0.89	**0.53**	0.68	0.77	0.59
DVI index 2	0.69	0.43	0.77	0.20	0.62	0.78	0.54	0.61	0.42	0.73	0.61	0.78	0.77	0.90	0.51	0.59	0.70	0.59
RVI index 2	0.82	0.38	0.78	0.24	0.52	0.80	0.55	0.53	0.65	0.86	0.57	0.81	0.86	0.84	0.49	0.56	0.76	0.61
NDVI index 2	0.82	0.38	0.78	0.24	0.52	0.80	0.56	0.53	0.65	0.86	0.57	0.81	0.86	0.84	0.49	0.56	0.76	0.61
SAVI index 2	0.82	0.38	0.78	0.24	0.53	0.80	0.56	0.53	0.65	0.86	0.57	0.81	0.86	0.84	0.49	0.56	0.76	0.61
MSAVI index 2	0.82	0.38	0.78	0.23	0.53	0.80	0.56	0.54	0.64	0.86	0.57	0.81	0.86	0.85	0.49	0.56	0.76	0.61
OSAVI index 2	0.82	0.38	0.78	0.24	0.52	0.80	0.56	0.53	0.65	0.86	0.57	0.81	0.86	0.84	0.49	0.56	0.76	0.61
DVI index 3	**0.91**	0.78	0.79	0.29	0.74	0.85	0.73	0.69	0.67	0.83	0.64	0.85	0.89	0.92	0.50	0.62	**0.84**	**0.62**
RVI index 3	0.75	0.64	0.79	0.24	0.76	0.74	0.68	0.69	0.43	0.64	0.64	0.79	0.78	0.91	0.52	0.60	0.71	0.57
NDVI index 3	0.75	0.66	0.79	0.23	0.75	0.75	0.69	0.71	0.41	0.63	0.64	0.79	0.78	0.92	0.52	0.60	0.70	0.56
SAVI index 3	0.76	0.66	0.79	0.23	0.75	0.75	0.69	0.71	0.42	0.64	0.64	0.79	0.78	0.92	0.52	0.61	0.70	0.56
MSAVI index 3	0.76	0.67	0.79	0.22	0.74	0.76	0.69	0.72	0.41	0.63	0.65	0.79	0.78	0.92	0.52	0.61	0.70	0.55
OSAVI index 3	0.76	0.66	0.79	0.23	0.75	0.75	0.69	0.71	0.41	0.63	0.64	0.79	0.78	0.92	0.52	0.60	0.70	0.56
DVI index 4	**0.91**	0.79	0.75	0.27	0.73	0.84	0.72	0.68	0.67	0.83	0.58	0.85	0.88	0.92	0.42	0.56	0.81	0.59
RVI index 4	0.74	0.64	0.77	0.22	0.75	0.71	0.67	0.69	0.41	0.64	0.62	0.77	0.76	0.92	0.47	0.59	0.71	0.57
NDVI index 4	0.74	0.66	0.76	0.21	0.74	0.73	0.67	0.71	0.40	0.63	0.62	0.78	0.75	0.92	0.47	0.60	0.70	0.56
SAVI index 4	0.74	0.66	0.77	0.21	0.74	0.73	0.67	0.71	0.40	0.63	0.62	0.78	0.76	0.92	0.47	0.60	0.70	0.56
MSAVI index 4	0.74	0.66	0.76	0.20	0.73	0.73	0.67	0.71	0.39	0.62	0.62	0.78	0.76	**0.93**	0.47	0.61	0.70	0.56
OSAVI index 4	0.74	0.66	0.76	0.21	0.74	0.73	0.67	0.71	0.40	0.63	0.62	0.78	0.75	0.92	0.47	0.60	0.70	0.56
Derivatives																		
1st 496-520	0.90	0.69	0.58	0.20	0.24	0.55	0.70	0.78	0.48	0.34	0.50	0.87	0.70	-0.51	0.45	0.55	0.82	0.52
1st 670-742	0.90	0.78	0.77	0.30	0.75	0.84	0.73	0.68	0.65	0.82	0.62	0.85	0.88	0.92	0.46	0.60	0.82	0.61
2nd 514-556	-0.90	-0.75	-0.80	-0.29	-0.63	**-0.86**	-0.72	-0.71	**-0.79**	-0.88	-0.62	**-0.89**	-0.90	-0.87	-0.48	-0.62	-0.82	**-0.62**
2nd 640-694	0.90	0.75	0.80	0.29	0.74	0.85	0.72	0.68	0.64	0.82	0.65	0.85	0.88	0.92	0.51	0.63	0.83	**0.62**
2nd 712-778	-0.89	-0.74	-0.79	**-0.31**	**-0.77**	-0.82	-0.74	-0.69	-0.59	-0.79	-0.65	-0.84	-0.85	-0.91	-0.52	-0.62	-0.81	-0.61